

AN ADAPTIVE SURROGATE MODELING BASED ON DEEP NEURAL NETWORKS FOR LARGE-SCALE BAYESIAN INVERSE PROBLEMS

LIANG YAN AND TAO ZHOU

ABSTRACT. It is popular approaches to use surrogate models to speed up the computational procedure for Bayesian inverse problems (BIPs). For instance, the polynomial chaos expansions (PCE) are often combined with the Markov chain Monte Carlo sampling to accelerate the online computations. While this approach can be very efficient, there exist, however, two main limitations: (i) the PCE surrogate admits limitations to handle problems with low regularity; (ii) the PCE surrogate suffers from the so called curse of dimensionality. To this end, we present in this work an adaptive multi-fidelity deep neural networks (DNNs) based surrogate modeling for large-scale BIPs, motivated by the facts that the DNNs can potentially handle functions with limited regularity and are powerful tools for high dimensional problems. More precisely, we begin with a low fidelity DNN-surrogate and then correct it adaptively using online high fidelity data. The key idea is to view the low fidelity surrogate as an input variable into the DNN-surrogate of the next iteration – yielding a composite DNN that combine two surrogates between two iterations. By doing this, the online correction procedure can be made very efficient. Numerical experiments confirm that the proposed approach can obtain accurate posterior information with limited number of forward simulations.

1. INTRODUCTION

Inverse problems arise when one is interested in determining model parameters or inputs from a set of indirect observations [6, 13]. Typically, inverse problems are often ill-posed in the sense that the solution may not exist or may not be unique. More importantly, the parameters may not depend continuously on the observations – meaning that one loses the stability. The Bayesian approach [13, 29] is a popular approach for inverse problems, and it casts the solution as a *posterior distribution* of the unknowns conditioned on observations, and introduces regularization in the form of *prior* information. By estimating statistic moments according to the posterior distribution, one not only gets point estimates of the parameters, but also obtains a complete description of the uncertainty in model predictions. However, in practice, the analytical treatment for posterior is not possible in general due to the complexity of the system. Consequently, the posterior is often approximated with numerical approaches such as the Markov chain Monte Carlo (MCMC) method.

In the standard MCMC approach, one aims at generating samples directly from the posterior distribution over the parameters space by using the unnormalized posterior, i.e., the product of the prior and likelihood. However, the cost of evaluating the likelihood in the

Date: June 10, 2019.

Department of Mathematics, Southeast University, Nanjing, China. Email: yanliang@seu.edu.cn. L. Yan is supported by NSF of China (No.11771081), the science challenge project (No. TZ2018001), Qing Lan project of Jiangsu Province and Zhishan Young Scholar Program of SEU.

LSEC, Institute of Computational Mathematics, Academy of Mathematics and Systems Science, Chinese Academy of Sciences, Beijing 100190, China. Email: tzhou@lsec.cc.ac.cn. T. Zhou is partially supported the NSFC (under grant numbers 11822111, 11688101, and 11731006), the science challenge project (No. TZ2018001), NCMIS, and the youth innovation promotion association (CAS).

sampling procedure can quickly become prohibitive if the forward model is computationally expensive. One popular way to reduce the computational cost in the sampling procedure is to replace the original forward model with a cheap surrogate model [8, 12, 14, 17, 18, 21, 22, 23, 30, 35]. Using a computational less expensive, offline constructed, surrogate model can make the online computations very efficient. Furthermore, theoretical analysis shows that if the surrogate converges to the true model in the prior-weighted L_2 norm, then the posterior distribution generated by the surrogate converges to the true posterior [23, 30, 35, 36].

Although the surrogate approach can provide significant empirical performance improvements, there are however many challenges for practical applications. First, constructing a sufficiently accurate surrogate over the whole domain of the prior distribution may not be possible for many practical problems [16]. Especially, the posterior often concentrates on a small fraction of the whole parameter domain, and a globally prior-based surrogate may not be accurate for online computations. To improve this, posterior-focused approaches have been suggested recently, where one constructs a sequence of local surrogates in the important region of the posterior distribution, to alleviate the effect of the concentration of posterior [4, 5, 16].

In our previous work [38], we also presented an adaptive multi-fidelity surrogate modelling procedure based on PCEs to speed up the online computations via MCMC. The idea is to begin with a low fidelity PCE-surrogate, and then correct it adaptively using online high fidelity data. Empirical studies on problems of moderate dimension show that the number of high-fidelity model evaluations can be reduced by orders of magnitude, with no discernible loss of accuracy in posterior expectations. Nevertheless, the approaches in [38] also admit some limitations: (i) the PCE surrogate has limitations to handle problems with low regularity; (ii) the PCE surrogate suffers from the so called curse of dimensionality. This motivate the present work: we shall present an adaptive multi-fidelity deep neural networks (DNNs) based surrogate modeling for large-scale BIPs, motivated by the facts that DNNs can potentially handle functions with limited regularity and are powerful tools for approximating high dimensional problems ([10, 26, 28, 32, 40]). The key idea is to view the low fidelity surrogate as a input variable into the DNN surrogate of the next iteration – yielding a composite DNNs that combine two surrogates between two iterations. Another key issue is to adaptively correct the DNN-surrogate locally so that the new surrogate is refined on a more concentrated (posterior) region in the parameter space. By doing this, one can perform the online correction procedure in a very efficient way. We shall present numerical experiments to show the effectiveness of the new approach. To the best of our knowledge, this is the first investigation of the multi-fidelity DNN-surrogate for Bayesian inverse problems.

The rest of the paper is organized as follows. In Section 2, we present some preliminaries and provide with a mathematical description of the BIPs. The adaptive multi-fidelity DNNs-surrogate approach is discussed in Section 3. In Section 4, we use a benchmark elliptic PDE inverse problem to demonstrate the accuracy and efficiency of our approach. Finally, we give some concluding remarks in Section 5.

2. BACKGROUND AND PROBLEM FORMULATION

In this section, we shall review some basic ideas for the surrogate-based approach in Bayesian inverse problems.

2.1. Bayesian inverse problems. We consider a discretized system of a mathematical model (such as PDEs) of interest:

$$(1) \quad F(u_h(z), z) = 0,$$

where $u_h(z) : \Xi \rightarrow \mathbb{R}^{n_h}$ is the discrete solution with n_h being the dimension of the finite-dimensional discretization in the physical domain, and $z \in \Xi \subset \mathbb{R}^n$ is a n -dimensional parameter vector. The discrete operator F denotes a numerical approximation, e.g., by the finite element or finite difference method for PDEs. The goal of an inverse problem is to estimate the unknown parameter vector z from noisy observations of the states u_h given by

$$(2) \quad d = g(u_h; z) + \xi.$$

Here g is a discretized observation operator mapping from the states and parameters to the observable, and $\xi \in \mathbb{R}^m$ is the measurement error (or the noise). The system model (1) together with the observation model (2) define a forward model $y = f(z)$ that maps the unknown parameter to the observable data.

To formulate the inverse problem in a Bayesian framework, we model the parameter z as a random variable (vector), and endow it with a prior distribution $\pi(z)$. The distribution of the z conditioned on the data d , i.e., the posterior distribution $\pi(z|d)$ follows the Bayes' rule:

$$\pi(z|d) \propto \mathcal{L}(z|d, f)\pi(z).$$

In case the density information of the $\xi \sim p_\xi$ is given, it follows directly that the likelihood function can be written as:

$$(3) \quad \mathcal{L}(z|d, f) = p_\xi(d - f(z)).$$

Notice that each evaluation of the likelihood function \mathcal{L} requires an evaluate of the forward model f . Thus, in sampling schemes such as the MCMC approach one has to perform $\sim 10^5$ forward model simulations, and this is a great challenge if the forward model f represents a large-scale computer model. Consequently, it is popular approach to construct (in a offline procedure) a cheaper surrogate for the forward model, and use it for online computations.

2.2. Surrogate-based Bayesian inference. Surrogate-based Bayesian inference has received much attention in recently years [7]. In this approach, one usually generate a collection of model evaluations (snapshots) $\mathcal{D} := \{(z, f(z))\}$, and then construct an approximation \tilde{f} based on those snapshots. Using this approximation \tilde{f} , one can obtain an approximated surrogate posterior

$$\tilde{\pi}(z|d) \propto \mathcal{L}(z|d, \tilde{f})\pi(z).$$

Under certain assumptions, the posterior distribution induced by the surrogate model \tilde{f} converges to the true posterior with respect to the Kullback-Leibler divergence [23, 35, 36]. If the evaluation of the approximation \tilde{f} is inexpensive, then the approximate posterior density $\tilde{\pi}$ can be evaluated for a large number of samples, without resorting to additional simulations of the forward model f .

Although the surrogate-based Bayesian inference procedure can be quite effective, the big challenge is that in high-dimensional parametric spaces, the number of training points used to build the surrogate (such as the PCE approach) grows fast with respect to the dimension, and this is known as the *curse of dimensionality*. To improve this, we shall introduce in the next section a deep neural networks based surrogate modeling which can potentially handle high dimensional Bayesian inference problems.

3. AN ADAPTIVE MULTI-FIDELITY DNN-BASED SURROGATE MODELING

In this section, we shall present an adaptive multi-fidelity DNN-based surrogate modeling for Bayesian inverse problems.

3.1. Feedforward DNN-based surrogate modeling. The basic idea of deep neural networks (DNNs) for surrogate modeling is that one can approximate an input-output map $f : \mathbb{R}^n \rightarrow \mathbb{R}^m$ through a hierarchical abstract layers of latent variables [9]. A typical example is the feedforward neural network, which is also called multi-layer perceptron (MLP). It consists of a collection of layers that include an input layer, an output layer, and a number of hidden layers. The size of the input layer and output layer are fixed and determined by the dimensionality of the input and output. Figure 1 illustrates the structure of a DNN with two hidden layers. Each circle in the schematic of the DNN is a neuron which calculates a weighted sum of an input vector plus bias and applies a non-linear function to produce an output. Specifically, given a n -dimensional input row vector $z \in \mathbb{R}^n$, we can define a DNN with L hidden layers as following

$$\mathcal{N}(z) = (S \circ A \circ F_{L-1} \circ \cdots \circ F_0)(z),$$

where $F_k : \mathbb{R}^{d_k} \rightarrow \mathbb{R}^{d_{k+1}}, k = 0, \dots, L-1$ are nonlinear maps, $A : \mathbb{R}^{d_L} \rightarrow \mathbb{R}^m$ is an affine map, and d_k is the number of neurons in the k th hidden layer. The choice of S is depends on the learning task. For instance, in regression tasks, the identity function is normally employed.

Let k be the index for layers, then the DNNs generate the following approximation $\mathcal{N}(z)$:

$$\begin{aligned} z^{(k+1)} &= \sigma(\mathbf{W}^{(k)} z^{(k)} + \mathbf{b}^{(k)}), \quad k = 0, \dots, L-1, \\ \mathcal{N}(z) &= \mathbf{W}^{(n)} z^{(n)} + \mathbf{b}^{(n)}. \end{aligned}$$

Here $\mathbf{W}^{(k)} \in \mathbb{R}^{d_{k+1} \times d_k}$, $\mathbf{b}^{(k)} \in \mathbb{R}^{d_{k+1}}$ are the weights and biases of the network, and σ is the activation function. Some popular choices for the activation function include sigmoid, hyperbolic tangent, rectified linear unit (ReLU), to name a few [9, 27]. In the current work, we shall use Swish as the activation function [27, 32]:

$$\sigma(z) = \frac{z}{1 + \exp(-z)}.$$

Once the network architecture is defined, one can resort to optimization tools to find the unknown parameters $\theta = \{\mathbf{W}^{(k)}, \mathbf{b}^{(k)}\}$ based on the training data. Precisely, let $\mathcal{D} := \{(z_i, y_i)\}_{i=1}^N$ be a set of training data, we can define the following minimization problem:

$$(4) \quad \arg \min_{\theta} \frac{1}{N} \sum_{i=1}^N \|y_i - \mathcal{N}(z_i; \theta)\|^2 + \lambda \Omega(\theta),$$

where $\mathcal{J}(\theta; \mathcal{D}) = \frac{1}{N} \sum_{i=1}^N \|y_i - \mathcal{N}(z_i; \theta)\|^2 + \lambda \Omega(\theta)$ is the so called loss function, $\Omega(\theta)$ is a regularizer and λ is the regularization constant. For our case, the regularizer $\Omega(\theta) = \frac{1}{2} \|\theta\|^2$. In practice, the averaging in Eq.(4) is performed over a small randomly sampled subset $\mathcal{D}_M \subset \mathcal{D}$, at each iteration of the optimization procedure. Solving this problem is generally via the stochastic gradient descent (SGD) algorithm [3]. SGD simply minimizes the function by taking a negative step along an estimate of the gradient $\nabla_{\theta} \mathcal{J}(\theta; \mathcal{D}_M)$ at iteration k . The gradients are usually computed through backpropagation. At each iteration, SGD updates the solution by

$$\theta_{k+1} = \theta_k + \epsilon \nabla_{\theta} \mathcal{J}(\theta; \mathcal{D}_M),$$

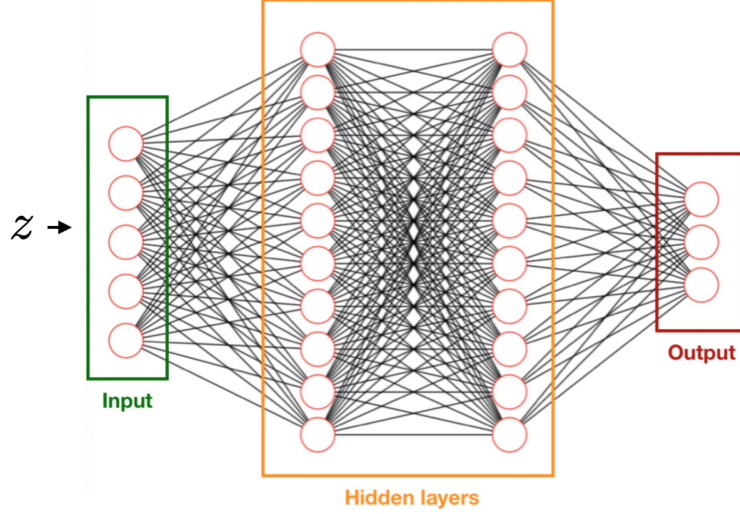


FIGURE 1. The structure of a two-hidden-layer neural network. The first column of nodes (from left to right) is the input layer, taking a d -dimensional vector z as input, and the last column is the output layer that generate a m -dimension output y . The intermediate columns are the hidden layers.

Algorithm 1 Multi-fidelity Composite Deep Neural Networks

Require: The low-fidelity model $\mathcal{N}^L(z)$; the high-fidelity model $f^H(z)$;

- 1: Choose additional training samples $\{z_k\}_{k=1}^Q$
 - 2: Run the low-fidelity model \mathcal{N}^L and high-fidelity model f^H for each z_k to obtain $\mathcal{N}^L(z_k)$ and $f^H(z_k)$.
 - 3: Train the new neural network $\mathcal{N}^H(z; \theta)$ with the training data $\left\{ \left((z_k, \mathcal{N}^L(z_k)), f^H(z_k) \right) \right\}_{k=1}^Q$ with Adam algorithm.
-

where ϵ is the learning rate. Recent algorithms that offers adaptive learning rates are available, such as Ada-Grad [39], RMSProp [31] and Adam [15], ect. The present work adopts Adam optimization algorithm.

It is clear that after obtaining the parameters θ , we have an explicit functional form $\mathcal{N}(z; \theta)$. This approximation can be then substituted into the computation procedure of the surrogate posterior, such as in the MCMC framework. However, we remark that a prior based surrogate might not be enough for online computations, see. e.g. [20, 38]. Thus, one usually needs to combine the surrogate with additional high fidelity data, yielding a multi-fidelity approach. To this end, we shall present in the next section an adaptive multi-fidelity DNN-surrogate modeling to accelerate the solution of BIPs.

3.2. An adaptive multi-fidelity DNN surrogate. In this section, we shall present an adaptive multi-fidelity DNN-based surrogate for BIPs. In particular, we consider to combine our approach within the MCMC framework, and extensions to general approaches such as Ensemble Kalman inversion [11, 37] or RTO [1, 33] are also possible. Our approach is motivated by recent works such as [19, 24], where composite DNNs are discussed to deal with multi-fidelity data.

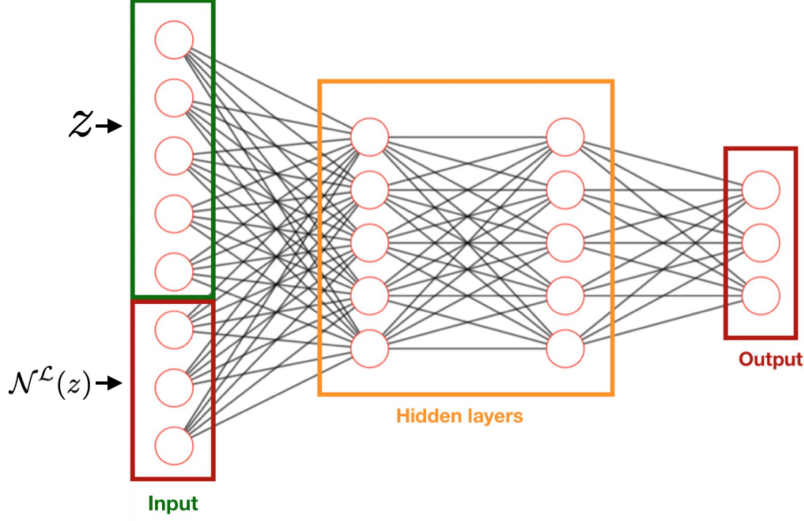


FIGURE 2. A composite architecture of DNN that combine a low fidelity DNN. The input is the concatenation of the parameter vector z and the low-fidelity data $\mathcal{N}^L(z)$, and the output is an updated DNN.

The main idea here is to discover and exploit the correlations between low- and high-fidelity data [25]. Suppose we have a high-fidelity model f^H (here we simply assume that f^H is the true forward model f) and a low-fidelity surrogate f^L (e.g., a trained DNN-surrogate \mathcal{N}^L in our framework). Then, we aim at learning a nonlinear map \mathcal{F} between the two models:

$$(5) \quad f^H(z) = \mathcal{F}(z, f^L(z)) = \mathcal{F}(z, \mathcal{N}^L(z)).$$

This can be done by approximating the nonlinear map \mathcal{F} using DNNs, i.e.,

$$(6) \quad f^H(z) \approx \mathcal{N}^H(z; \theta) := \mathcal{N}(z, \mathcal{N}^L(z); \theta).$$

The new involved parameters θ can be trained by using additional high fidelity data $\left\{ \left((z_k, \mathcal{N}^L(z_k)), f^H(z_k) \right) \right\}_{k=1}^Q$, and this yields a composite DNNs as illustrated in Fig. 2.

The key idea here is to view the low-fidelity model \mathcal{N}^L as an input into the high fidelity DNN, motivated by the fact that models are highly correlated. By doing this, one can expect to use fewer layers (or even use a shallow neural network) for constructing \mathcal{N}^H – resulting much reduced computational complexity in the training procedure. The detailed step for constructing \mathcal{N}^H are summarized in Algorithm 1.

At this stage, one may ask why not just include those additional high fidelity data $\left\{ \left((z_k, f^H(z_k)) \right) \right\}_{k=1}^Q$ when training \mathcal{N}^L (–yielding a better surrogate)? The answer is that, in the beginning, one can only construct the surrogate with prior-based information, and this surrogate may not be enough even if large sample evaluations are used, as the posterior density will in general concentrate to a small region. Thus, we aim at adaptively correct the surrogate online using local data. Details will be presented in the next section.

REMARK. We close this section by remarking that in [38], a correction procedure for the PCE-based surrogate is discussed. In particular, the following correction technique is

presented:

$$(7) \quad f^H(z) \approx f_{\text{PCE}}^H(z) := f_{\text{PCE}}^L(z) + f_{\text{CORR}}(z),$$

where $f_{\text{PCE}}^L(z)$ is the low-fidelity PCE-surrogate, and $f_{\text{CORR}}(z)$ is the correction term that is determined online by additional high fidelity data. Notice that this is a *linear* correction, as f_{PCE}^H and f_{PCE}^L are linearly dependent. While in the present work, the correction procedure (5)-(6) can learn a nonlinear correlation between models (which is in general the case for practical applications).

3.3. An adaptive procedure for correcting the surrogate. We now propose an adaptive procedure to correct the surrogate in the MCMC framework. The procedure begins with a low fidelity model \mathcal{N}^L that is constructed offline. Then, for the online computations, an adaptive sampling framework is used to construct and refine the surrogate model, following the idea in our previous work [38]. The procedure consists of the following steps:

- Initialization: build a low fidelity model \mathcal{N}^L . Set $f^L = \mathcal{N}^L$.
- Online computations: using the surrogate f^L , run the MCMC algorithm to sample the approximated posterior distribution for a certain number of steps (say 1000 steps). The last state z^- will be used to propose a candidate z^+ .
- Indicator for refinement: generate an accept sample y using high fidelity information on z^- and z^+ . Then compute the difference between the high fidelity model f^H and the surrogate f^L at y . If the difference is bigger than a given tolerance, then one generates new high fidelity data to correct the model \mathcal{N}^H using Algorithm 1. Set \mathcal{N}^H as the new surrogate, i.e., $f^L = \mathcal{N}^H$.
- Use the surrogate f^L to accept/reject the proposal z^+ .
- Repeated the above procedure for many times (say at most I_{\max} times). Finally the posterior samples can be generated by gathering all the samples in the above procedures.

Choosing the indicator for correcting the surrogate f^L is the most critical issue in the above procedure. As mentioned, we first sampling approximate posterior distribution based on the surrogate model f^L for a certain number of steps using a standard Metropolis-Hastings (MH) algorithm. The goal is to generate several samples that the initial sample points and the last point are uncorrelated. Similar to the MH algorithm, we compute an acceptance probability using the high fidelity model f^H (or the true forward model):

$$(8) \quad \beta = \min \left\{ 1, \frac{\mathcal{L}(d, f^H(z^-))\pi(z^-)}{\mathcal{L}(d, f^H(z^+))\pi(z^+)} \right\}.$$

Using this parameter β , we can obtain an accept point y , which is expected to be much closer to the posterior region.

Once we obtain the accept candidate point y , we then compute the relative error

$$(9) \quad \text{err}(y) = \frac{\|f^H(y) - f^L(y)\|_\infty}{\|f^H(y)\|_\infty}.$$

If this error indicator exceeds a user-given threshold tol , we shall generate Q random points $\{z_i\}_{i=1}^Q$ locally around y (say, uniformly sampling in a local ball $B(y, R) := \{z : \|z - y\|_\infty \leq R\}$) to correct the surrogate model f^L using Algorithm 1. While if the error indicator is smaller than tol , it means that the low-fidelity model is still acceptable and we just go ahead. The detailed procedure for updating the surrogate model is summarized in Algorithm 2.

In the correction procedure, we can not afford too many high fidelity simulations, that is, Q can not be too large. Consequently, to avoid over fitting for the online training procedure,

Algorithm 2 Indicator for correcting the surrogate

Require: Set an error threshold tol and the radius R . Given z^- and z^+ , we do the following steps:

- 1: Compute acceptance probability using high-fidelity model f^H

$$\beta = \min \left\{ 1, \frac{\mathcal{L}(d, f^H(z^-))\pi(z^-)}{\mathcal{L}(d, f^H(z^+))\pi(z^+)} \right\}$$

- 2: Draw $s \sim \mathcal{U}(0, 1)$. If $s < \beta$, let $y = z^-$, otherwise $y = z^+$.
 - 3: Compute the relative error $err(y)$ using Eq. (9)
 - 4: **if** $err(y) > \epsilon$ **then** we generate Q random points locally $\{z_i\} \in B(y, R)$ and correct the surrogate model to get $\mathcal{N}^H(z)$ using Algorithm 1
 - 5: **end if**
 - 6: **return** Set $\mathcal{N}^H(z)$ as the new low-fidelity surrogate model.
-

we limit ourselves to use a DNN with at most two hidden layers (or even consider shallow networks). Algorithm description of the MH approach using locally adapted multi-fidelity DNN-surrogate is summarized in Algorithm 3.

Algorithm 3 Adaptive multi-fidelity DNN-based MH algorithm

Require: Given the initial surrogate $f^L = \mathcal{N}^L$ and a proposal density q , we fix a stopping indicator m for the MCMC sampling, i.e., we shall stop to check if the correction is needed for each m -steps, for instance, we can choose $m = 1000$. We also set a maximum number I_{max} of corrections, that is, we shall at most correct the surrogate for I_{max} time so that one can control the total computational complexity.

- 1: Choose a starting points z_0 ; let $X_0 = \{\}$;
- 2: **for** $n = 1, \dots, I_{max}$ **do**
- 3: Draw $m - 1$ samples $\{z_1, \dots, z_{m-1}\}$ from the approximate posterior based on f^L . Propose $z^* \sim q(\cdot | z_{m-1})$.
- 4: If the surrogate needs refinement near z^* or z_{m-1} , then select new samples locally to correct the surrogate to get \mathcal{N}^H using Algorithm 2. Set $f^L = \mathcal{N}^H$.
- 5: Compute acceptance probability

$$\alpha = \min \left(1, \frac{\mathcal{L}(d, f^L(z^*))\pi(z^*)}{\mathcal{L}(d, f^L(z_{m-1}))\pi(z_{m-1})} \right)$$

- 6: Draw $s \sim \mathcal{U}(0, 1)$. If $s < \alpha$, let $z_m = z^*$, otherwise $z_m = z_{m-1}$.
 - 7: Let $z_0 = z_m$ and $X_n = X_{n-1} \cup \{z_1, \dots, z_m\}$
 - 8: **end for**
 - 9: **return** Posterior samples $X_{I_{max}}$
-

To summary, our approach departs from an offline constructed DNN-surrogate, and then we correct the multi-fidelity DNN-surrogate adaptively using locally generated high fidelity data. The key idea is to consider the composite DNNs in which the previous trained DNN model \mathcal{N}^L is viewed as an input variable in the next updated surrogate. The locally generated training data are then expected to concentrate to the high probability region of the posterior density. The online training procedure is also expected to be efficient due to the correlation of two models.

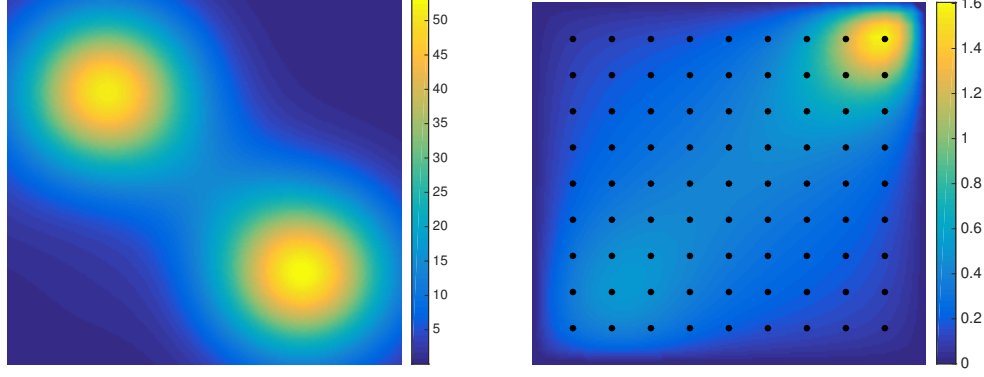


FIGURE 3. Example 1: Setup of the test case for Example 1. Left: the true permeability used for generating the synthetic data sets. Right: the model outputs of the true permeability. The figure is adopted from [38].

4. NUMERICAL EXAMPLES

In this section, we present a benchmark elliptic PDE inverse problem to illustrate the accuracy and efficiency of the proposed adaptive multi-fidelity DNN (ADNN) algorithm. We describe three examples in which ADNN algorithm produce accurate posterior samples using dramatically fewer evaluations of the forward model than the conventional MCMC. For each of these examples, we run the ADNN algorithm for $I_{max} = 50$ iterations, with subchain length $m = 1,000$. Unless otherwise specified, we shall use the following parameters $tol = 0.1, R = 0.2$ in ADNN. The learning rate was set $\epsilon = 10^{-3}$, and the hyper-parameter values of Adam were chosen based on default recommendations as suggested by [15]. To make a fair comparison, we run the prior-based DNN method described in Section 3.1 for 50,000 iterations. The MCMC simulation using the high-fidelity model is also conducted, and its results are used as the reference to evaluate accuracy and efficiency of the two methods. For both algorithms, the same fixed Gaussian proposal distribution is used, and the last 30,000 realizations are used to compute the relevant statistical quantities. All the computations were performed using MATLAB 2015a on an Intel-i5 desktop computer.

4.1. Problem setup. We consider the problem of inferring subsurface permeability from a finite number of noisy pressure head measurements [5, 38]. More specifically, consider a domain of interest $\Omega = [0, 1]^2$, and let $u(x)$ be pressure head, is the solution of an elliptic PDE in two spatial dimensions

$$(10) \quad \begin{aligned} -\nabla \cdot (\kappa(x) \nabla u(x)) &= f(x), \quad x \in \Omega, \\ u(x) &= 0, \quad x \in \partial\Omega. \end{aligned}$$

The data d is given by a finite set of u , perturbed by noise, and the problem is to recover the permeability $\kappa(x)$ from these measurements. In what follows, we choose the source $f(x) = 100 \sin(\pi x_1) \sin(\pi x_2)$.

In the numerical simulation, we solve the equation (10) using a spectral approximations with polynomial degree $P = 6$. In order not to commit an 'inverse crime', we generate the data by solving the forward problem using a higher order ($P=10$) than that is used in the inversion.

4.2. Example 1: a nine-dimensional inverse problem. In the first example, the permeability field $\kappa(x)$ is defined by

$$\kappa(x) = \sum_{i=1}^9 \kappa_i \exp(-0.5 \frac{\|x - x_{0,i}\|^2}{0.15^2}),$$

where $\{x_{0,i}\}_{i=1}^9$ are the centers of the radial basis function, and the weights $\{\kappa_i\}_{i=1}^9$ are parameters in the Bayesian inverse problem.

This example is a typical benchmark problem considered in Refs. [5, 38] and it is investigated here for comparison purpose. To this end, we use the same model setup and synthetic data used in [38]. More precisely, the prior distributions on each of the weights $\kappa_i, i = 1, \dots, 9$ are independent and log-normal; that is, $\log(\kappa_i) \sim N(0, 1)$. The true parameter is drawn from $\log(\kappa_i) \sim U(-5, 5)$, and the true permeability field used to generate the test data is shown in Fig.3. The synthetic data d is generated by selecting the values of the states at a uniform 9×9 sensor network

$$d_j = u(x_j) + \max_j \{|u(x_j)|\} \delta \xi_j,$$

where δ dictates the relative noise level and ξ_j is a Gaussian random variable with zero mean and unit standard deviation. In the following, unless otherwise specified, we set $\delta = 0.05$.

4.2.1. Comparison of approximations. We compare the posterior approximations obtained by three types of approaches:

- The *conventional MCMC*, or the direct MCMC approach based on the forward model evaluations.
- The MCMC approach based on a prior-based DNN surrogate model evaluations.
- The ADNN approach presented in Section 3.

In our figure and results, we will use “Direct” to denote the conventional MCMC, “DNN” to denote the prior-based DNN approach, and “ADNN” to denote the ADNN algorithm. For the ADNN algorithm, we first construct a prior-based DNN surrogate \mathcal{N}^L using $N = 50$ training points with 4 hidden layers and 40 neurons per layer. Using this DNN model as low-fidelity model, we can construct and refine a multi-fidelity model \mathcal{N}^H via Algorithm 3. Especially, when the error indicator $err(y)$ exceeds the threshold tol , we choose $Q = 10$ random points in a local set $B(y, R)$ to refine the multi-fidelity NN surrogate \mathcal{N}^H . Here, one hidden layer with 50 neurons are used in \mathcal{N}^H . In this example, the regularization parameter λ is set to 0, i.e., no regularization is used.

To assess the sampling accuracy of the ADNN algorithm, Fig. 4 provides the marginal distributions of each component of the parameters, and the contours of the marginal distributions of each pair of components. The black lines represent the results generated by the direct MCMC approach based on the high-fidelity model evaluations (the reference solution), the red and blue lines represent results of the ADNN with $tol = 0.1$ and $tol = 0.05$, respectively. The plots in Fig. 4 suggest that the ADNN algorithm results in a good approximation to the reference solution. The conditional mean arising from ADNN algorithm and the direct MCMC approach are shown in Fig. 5. We observe that all algorithms produce similar estimates of mean in this test case. Furthermore, the results presented in Fig. 5 show clearly that our method also produces comparable accuracy as Ref. [38].

To verify the accuracy of our proposed algorithm, we also compute the posterior approximation obtained by the DNN-approach described in Section 3.1. In this case, the low-fidelity \mathcal{N}^L is built in advance and kept unchanged during MCMC computations. The conditional mean arising from the conventional MCMC and the DNN model with different

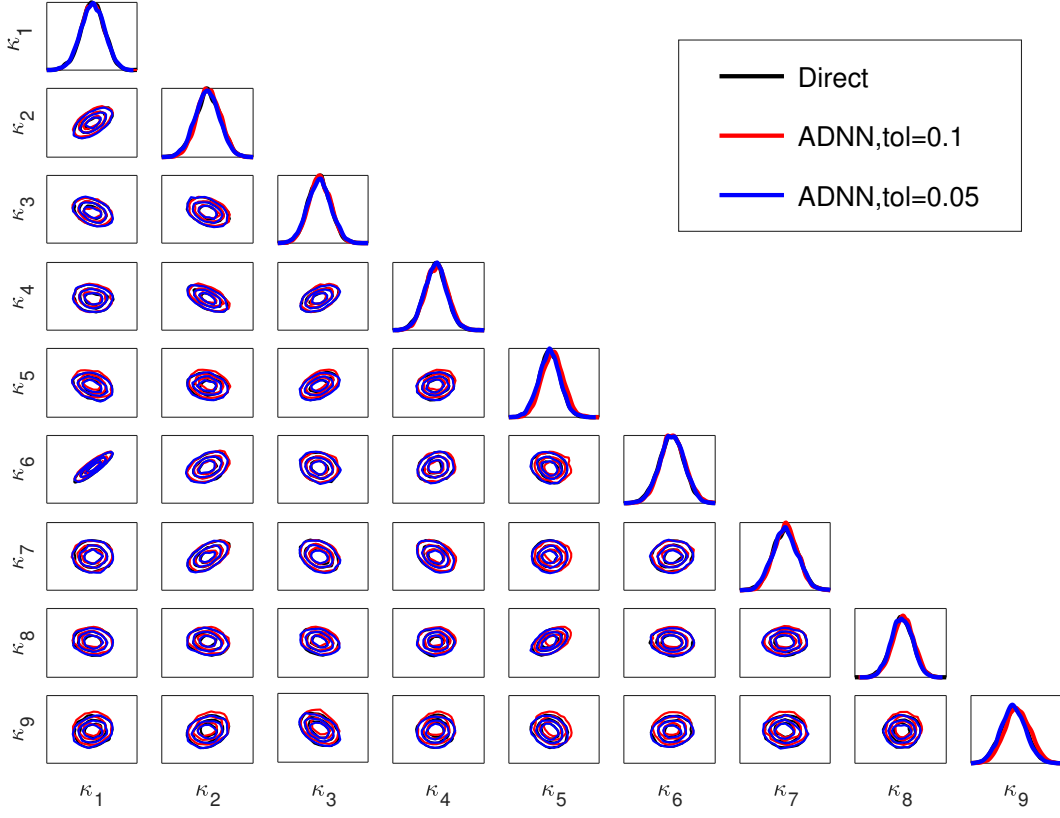


FIGURE 4. Example 1: One- and two-dimensional posterior marginals of the nine parameters. Black line: the Direct method. Red line: the ADNN algorithm with $tol = 0.1$; Blue line: the ADNN algorithm with $tol = 0.05$.

TABLE 1. Example 1. Computational times, in seconds, given by four different methods.

Method	Offline		Online		Total time(s)
	# of model evaluations	CPU(s)	# of model evaluations	CPU(s)	
Direct	—	—	5×10^4	1492.2	1492.2
DNN, $N = 50$	50	11.3	—	5.1	16.4
DNN, $N = 110$	110	12.7	—	5.1	17.8
ADNN, $N = 50$	50	11.3	300	31.9	43.2
ADNN, $N = 110$	110	12.7	180	18.4	31.1
AMPC, $N_C = 2$	110	2.9	1,010	38.7	41.6

sizes of the training dataset $N = \{50, 110\}$ are plotted in Fig. 6. Since the exact parameter is far from what is assumed in the prior, it is evident from the figure that the results using the prior-based DNN approach give a large error. By comparing Figs. 5 and 6, we can obtain that the approximation results using ADNN are much accurate than those using the prior-based DNN method.

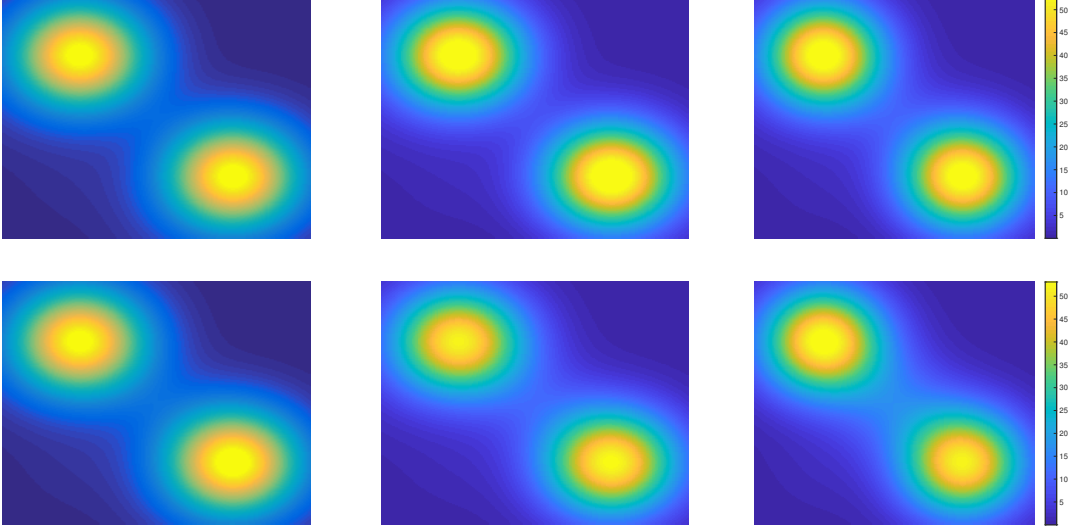


FIGURE 5. Example 1: (Left column) Conditional mean arising from direct MCMC. (Middle column) Conditional mean arising from ADNN ($tol = 0.1$). (Right column) Conditional mean arising from ADNN ($tol = 0.05$). From top to bottom, the relative noise level δ is 0.01, 0.05 respectively.

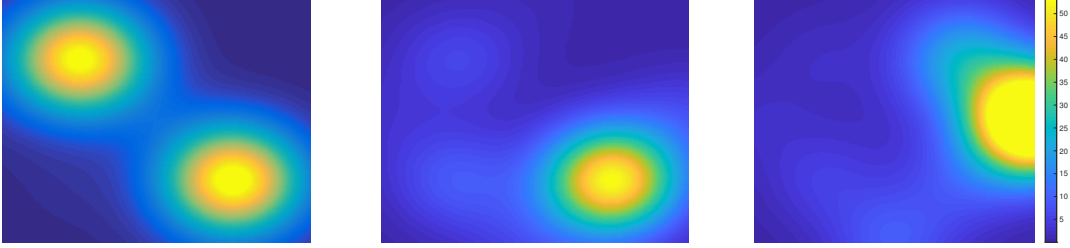


FIGURE 6. Example 1: (Left) Conditional mean arising from direct MCMC. (Middle) Conditional mean arising from prior-based DNN approach ($N=110$). (Right) Conditional mean arising from prior-based DNN approach ($N=50$).

The computational costs, given by three different algorithms, are shown in Table 1. Furthermore, we also show the results obtained by the adaptive multi-fidelity PC (AMPC) [38], which is noted to be similar as the results from the ADNN. The main computational time in the DNN-based algorithm is the offline model evaluations. Upon obtaining a trained DNN model \mathcal{N}^L , the online simulation is very cheap as it does not require any high-fidelity model evaluations. For the ADNN, we do need the online forward model simulations to construct and refine the multi-fidelity DNN model \mathcal{N}^H . Nevertheless, in contrast to 5×10^4 high-fidelity model evaluations in the conventional MCMC, the number of model evaluations for the ADNN with $N = \{50, 110\}$ are 300 and 180, respectively. As can be seen from the table, the ADNN algorithm can significantly improve the accuracy, yet without a dramatic increase in the computational time compared to the prior-based DNN method. The results

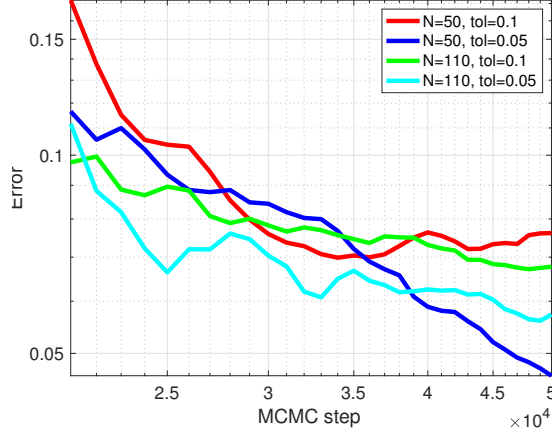


FIGURE 7. Example 1: The accuracy of ADNN using various numbers of the threshold tol .

using the AMPC is displayed in last column of Table 1. The number of model evaluations for the AMPC with an N_C -order ($N_C = 2$) correction expansion are 1010, which is much larger than the ADNN. In addition, the ADNN can be applied to high-dimensional cases, hence outperforming AMPC [38].

4.2.2. The influence of tuning parameters tol and R . Intuitively, one would expect the accuracy of the ADNN to improve as the value of the threshold tol decreases. To verify this proposition, we test several constant values choosing from $tol \in \{0.1, 0.05\}$ and $N \in \{50, 110\}$. With these settings, we run Algorithm 3 using the ADNN model. After discarding 2×10^4 burn-in samples for each chain, we consider the evolution of the error as the chain lengthens; we compute an error measure at each step $rel(k)$ defined as

$$rel(k) = \frac{\|\bar{\kappa} - \kappa^\dagger\|_\infty}{\|\kappa^\dagger\|_\infty},$$

where κ^\dagger are the “true” conditional mean arising from direct MCMC, and $\bar{\kappa}$ is the conditional mean arising from ADNN. Because the SGD for ADNN algorithm is random, we report the mean error over a size-10 ensemble of tests.

The accuracy comparison is given in Fig. 7, which shows the evolution of the relative error with the number of MCMC steps. The corresponding computational costs are summarized in Fig. 8, which shows the total number of high-fidelity model evaluations and CPU times performed for any given number of MCMC steps. As expected, the relative error decreases when threshold tol is smaller; these values trigger more frequent refinements. When refinement is set to occur at a very low rate, the resulting chain is inexpensive, and in contrast, smaller values of tol show increased cost and reduced errors. However, even using $N = 110, tol = 0.05$, the speedup over the direct method is quite dramatic. The time required by the conventional MCMC grows linearly with the number of samples. On the other hand, the ADNN requires a fixed amount of time at the initial cost, in order to train the prior-based DNN model, while the computational cost for new sample point is almost negligible. When the refinement is set to occur, the cost of the ADNN approach still grows, but very slowly. Indeed, the per-sample cost is sever orders of magnitude smaller for ADNN evaluations than for direct evaluations, and thus for even a moderate number of samples the gain in efficiency is significant.

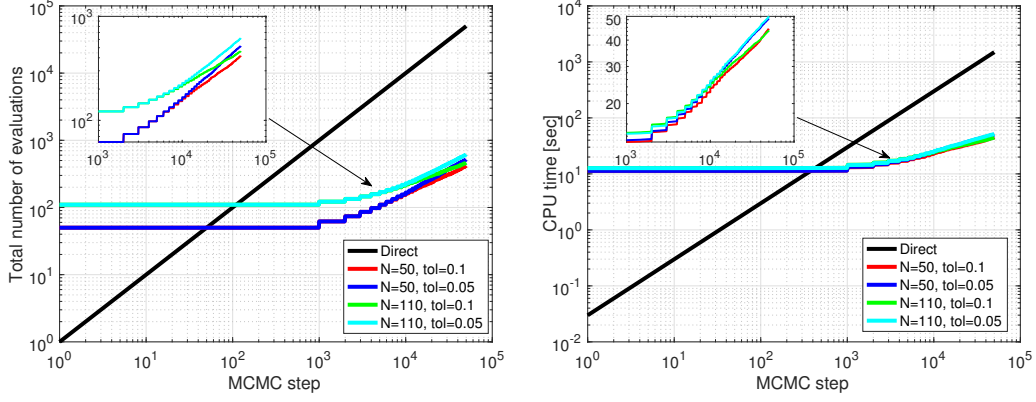


FIGURE 8. Example 1: The numerical results obtained using various numbers of the threshold tol .

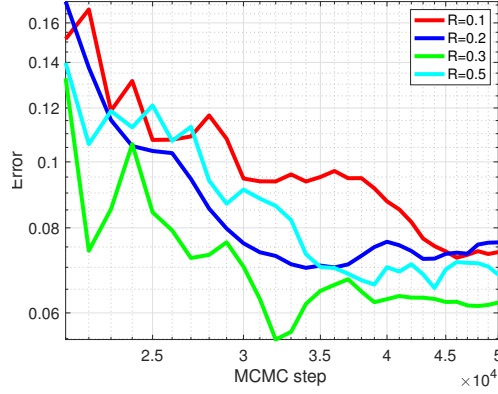


FIGURE 9. Example 1: The accuracy of ADNN using various values of the radius R .

Next, we investigate the sensitivity of the numerical results with respect to the radius R . The numerical results for Example 1, obtained using $N = 50, tol = 0.1$ and various values for the radius R are illustrated in Figs. 9 and 10. From the numerical results, we can conclude that the proposed scheme is relatively independent of the radius R .

4.3. Example 2. As the second example, the true parameter is a draw from the prior distribution described in Example 1. In other words, we consider the best-case-scenario where our prior knowledge includes the truth. The exact permeability used for generating the synthetic data and the reference solution arising the full model are displayed in Fig.11.

Similar to the first example, we numerically investigate the efficiency of the ADNN approach. Using the same setting as Example 1, we plot the conditional mean arising from different methods using various values of N . The numerical results obtained by DNN are shown in the left column of Fig.12. Compare with Fig. 6, it can be seen that the numerical results obtained by DNN using $N = 110$ training points agree with the reference solution. However, a smaller number of training points ($N = 50$) results a poor estimate. The corresponding results obtained by ADNN are also shown in Fig.12. It is clearly shown that the ADNN approach results in a very good approximation to the reference solution. Even with a

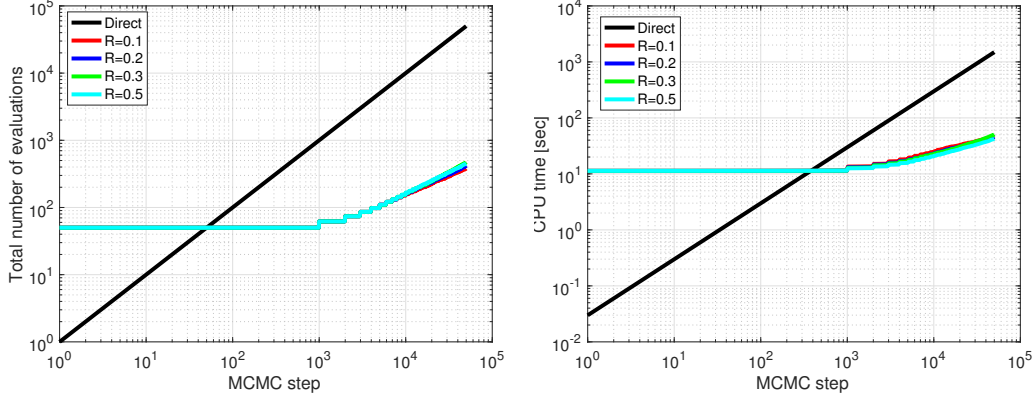


FIGURE 10. Example 1: The numerical results obtained using various numbers of the radius R .

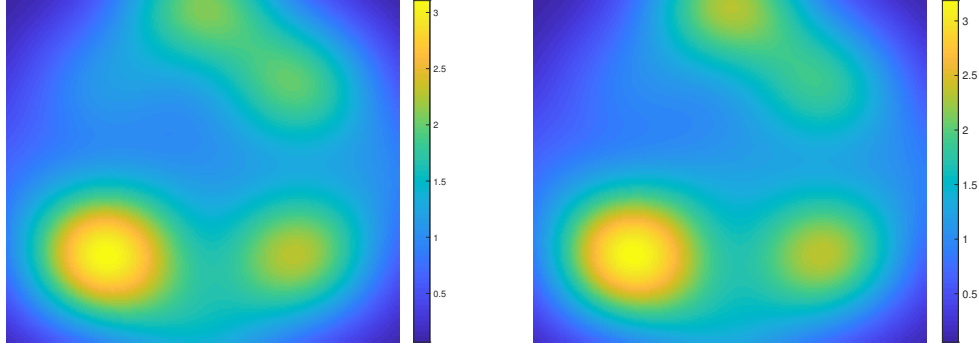


FIGURE 11. Example 2. Left: the true permeability used for generating the synthetic data set. Right: the reference solution arising the full model.

smaller $N = 50$ and a larger $tol = 0.1$, the ADNN approach admits a rather accurate result. The corresponding computational costs are summarized in Fig.13. Again, the online computing time required by ADNN and DNN is only a small fraction of that by the conventional MCMC. The accuracy comparison is summarized in the right of Fig.13. It can be seen from this figure that the ADNN offers a significant improvement in the accuracy, but does not significantly increase the computation time compared to the prior-based DNN approach. This also confirms the efficiency of the ADNN algorithm for this best-case-scenario.

4.4. Example 3: a high dimensional inverse problem. In the last example, we consider the permeabilities as a random field. Especially, the log-diffusivity field $\log \kappa(x) := p(x)$ is endowed with a Gaussian process prior, with mean zero and an isotropic kernel:

$$C(x_1, x_2) = \sigma^2 \exp \left(- \frac{\|x_1 - x_2\|^2}{2l^2} \right),$$

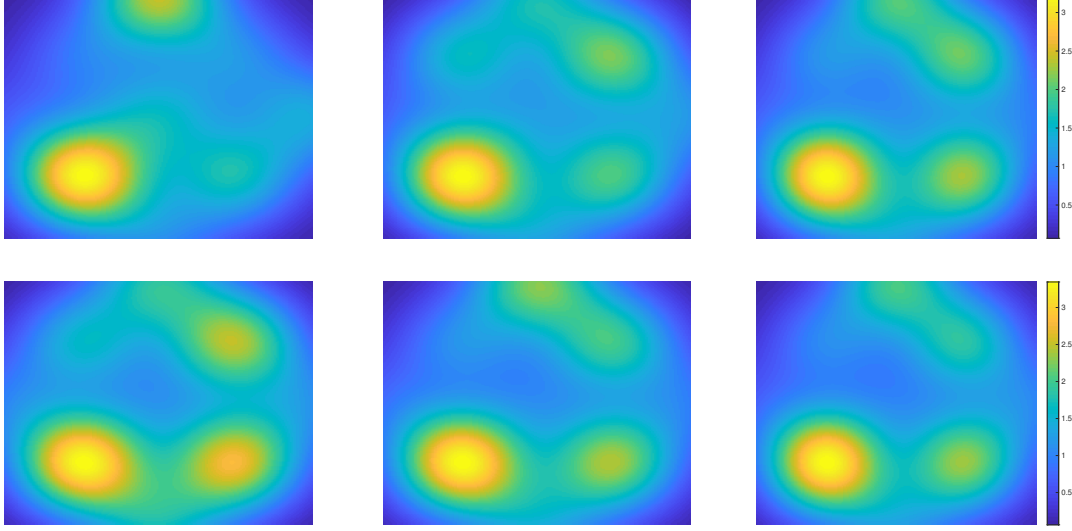


FIGURE 12. Example 2: (Left column) Conditional mean arising from DNN approach. (Middle column) Conditional mean arising from ADNN (tol=0.1). (Right column) Conditional mean arising from ADNN (tol=0.05). From top to bottom, the number of the training set N is 50, 110 respectively.

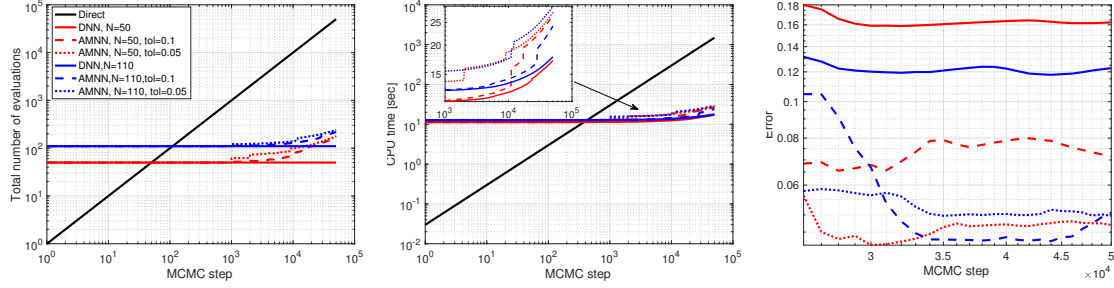


FIGURE 13. Example 2: The accuracy and cost of sampling using three methods.

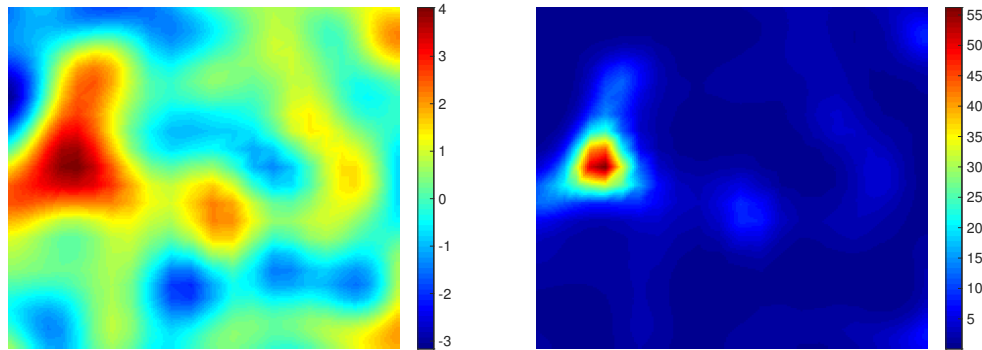


FIGURE 14. Example 3: The true solution $p(x)$ and $\kappa(x)$.

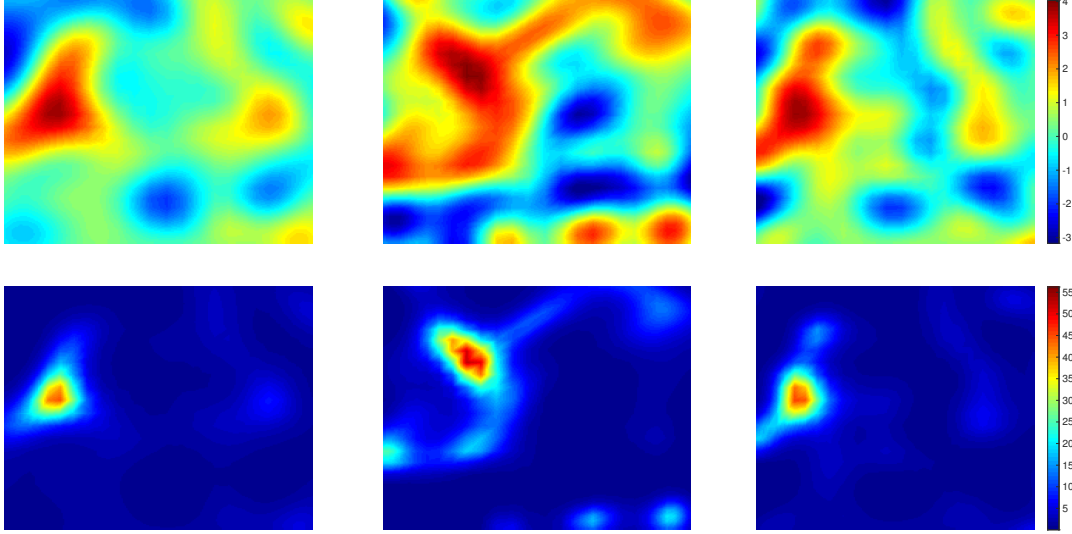


FIGURE 15. Example 3: (Left column) Conditional mean arising from direct MCMC. (Middle column) Conditional mean arising from prior-based DNN approach ($N = 100$). (Right column) Conditional mean arising from ADNN ($tol = 0.1$).

for which we choose variance $\sigma^2 = 1$ and a length scale $l = 0.1$. This prior allows the field to be easily parameterized with a Karhunen-Loeve expansion:

$$(11) \quad p(x; z) \approx \sum_{i=1}^n z^i \sqrt{\lambda_i} \phi_i(x),$$

where λ_i and $\phi_i(x)$ are the eigenvalues and eigenfunctions, respectively, of the integral operator on $[0, 1]^2$ defined by the kernel C , and the parameter $z = (z^1, \dots, z^n)$ are endowed with independent standard normal priors, $z^i \sim N(0, 1)$. These parameters then become the targets of inference. In particular, we truncate the Karhunen-Loeve expansion at $n = 111$ modes. The true solution $p(x)$ and $\kappa(x)$ used to generate the test data are shown in Fig.14. The measurement sensors of u are evenly distributed over Ω with grid spacing 0.1. The observational errors are taken to be additive and Gaussian:

$$d_j = u(x_j; z) + \xi_j,$$

with $\xi_j \sim N(0, 0.01^2)$. In this example, three hidden layers and 150 neurons per layer are used in \mathcal{N}^L , while 1 hidden with 150 neurons are used in \mathcal{N}^H . The regularization rate is set to $\lambda = 10^{-6}$. If the refinement is set to occur, we choose $Q = 50$ random points to train the multi-fidelity DNN \mathcal{N}^H .

Fig. 15 plots the conditional mean arising from three different approaches. As expected, a poor estimate is obtained by the prior-based DNN approach. The results are improved with the ADNN algorithm. The computational costs for the different algorithms are shown in Table 2. Building a DNN surrogate using $N = 100$ training points requires an offline CPU time of 26.81s, whereas its online evaluation requires 9.48s. On the other hand, for the ADNN algorithm with $tol = 0.1$, the offline and online CPU times are 26.81s and 88.92s,

TABLE 2. Example 3. Computational times, in seconds, given by three different methods.

Method	Offline		Online		Total time(s)
	# of model evaluations	CPU(s)	# of model evaluations	CPU(s)	
Direct	—	—	5×10^4	5507.5	5507.5
DNN	100	26.8	—	9.5	36.3
ADNN	100	26.8	950	88.9	115.7

respectively. This demonstrated that the ADNN can provide with much more accurate results, yet with less computational time.

5. SUMMARY

We have presented an adaptive DNN-based surrogate modelling procedure for Bayesian inference problems. Our approach begin with a low fidelity DNN-surrogate and then correct it adaptively online using high fidelity data. The key idea is to use multi-fidelity data for online computations, and view the trained DNN surrogate as an input variable in the surrogate (that will be updated) in the next iteration. By doing this, the online computation can be made in a very efficient way. The performance of the proposed strategy has been illustrated by three numerical examples. Although our approach has been presented in the MCMC framework, the idea can be easily extended to other approaches such as Sequential Monte Carlo (SCM)[2] or optimization-based sampling[1, 33, 34]. The extension of the present algorithm to Ensemble Kalman inversion[11, 37] is also straightforward.

REFERENCES

- [1] J. M. Bardsley, A. Solonen, H. Haario, and M. Laine. Randomize-then-optimize: A method for sampling from posterior distributions in nonlinear inverse problems. *SIAM Journal on Scientific Computing*, 36(4):A1895–A1910, 2014.
- [2] A. Beskos, A. Jasra, E. A Muzaffer, and A. M Stuart. Sequential monte carlo methods for bayesian elliptic inverse problems. *Statistics and Computing*, 25(4):727–737, 2015.
- [3] L. Bottou. Large-scale machine learning with stochastic gradient descent. In *Proceedings of COMP-STAT’2010*, pages 177–186. Springer, 2010.
- [4] P. R. Conrad, Y. M. Marzouk, N. S. Pillai, and A. Smith. Accelerating asymptotically exact MCMC for computationally intensive models via local approximations. *Journal of the American Statistical Association*, 111(516):1591–1607, 2016.
- [5] T. Cui, Y. M. Marzouk, and K. Willcox. Data-driven model reduction for the Bayesian solution of inverse problems. *International Journal for Numerical Methods in Engineering*, 102(5):966–990, 2015.
- [6] S. N. Evans and P. B. Stark. Inverse problems as statistics. *Inverse Problems*, 18(4):R55–R97, 2002.
- [7] M. Frangos, Y. Marzouk, K. Willcox, and B. van Bloemen Waanders. Surrogate and reduced-order modeling: a comparison of approaches for large-scale statistical inverse problems. *Biegler, L. and Biros, G. and Ghattas, O. and Heinkenschloss, M. and Keyes, D. and Mallick, B. and Marzouk, Y. and Tenorio, L. and van Bloemen Waanders, B. and Willcox, K. editors, Computational Methods for Large Scale Inverse Problems and Uncertainty Quantification, John Wiley & Sons, UK*, pages 123–149, 2010.
- [8] D. Galbally, K. Fidkowski, K. Willcox, and O. Ghattas. Non-linear model reduction for uncertainty quantification in large-scale inverse problems. *International Journal for Numerical Methods in Engineering*, 81(12):1581–1608, 2010.
- [9] I. Goodfellow, Y. Bengio, and A. Courville. *Deep learning*. MIT press, 2016.
- [10] J. Han, A. Jentzen, and W. E. Solving high-dimensional partial differential equations using deep learning. *Proceedings of the National Academy of Sciences*, 115(34):8505–8510, 2018.
- [11] M. A. Iglesias, K. JH Law, and A. M. Stuart. Ensemble kalman methods for inverse problems. *Inverse Problems*, 29(4):045001, 2013.

- [12] B. Jin. Fast Bayesian approach for parameter estimation. *International Journal for Numerical Methods in Engineering*, 76(2):230–252, 2008.
- [13] J. P. Kaipio and E. Somersalo. *Statistical and Computational Inverse Problems*, volume 160. Springer, 2005.
- [14] M. C Kennedy and A. O’Hagan. Bayesian calibration of computer models. *Journal of the Royal Statistical Society: Series B (Statistical Methodology)*, 63(3):425–464, 2001.
- [15] D. Kingma and J. Ba. Adam: A method for stochastic optimization. *arXiv preprint arXiv:1412.6980*, 2014.
- [16] J. Li and Y. M Marzouk. Adaptive construction of surrogates for the Bayesian solution of inverse problems. *SIAM Journal on Scientific Computing*, 36(3):A1163–A1186, 2014.
- [17] W. Li and G. Lin. An adaptive importance sampling algorithm for Bayesian inversion with multimodal distributions. *Journal of Computational Physics*, 294:173–190, 2015.
- [18] C. Lieberman, K. Willcox, and O. Ghattas. Parameter and state model reduction for large-scale statistical inverse problems. *SIAM Journal on Scientific Computing*, 32(5):2523–2542, 2010.
- [19] C. Lu and X. Zhu. Bifidelity data-assisted neural networks in nonintrusive reduced-order modeling. *arXiv preprint arXiv:1902.00148*, 2019.
- [20] F. Lu, M. Morzfeld, X. Tu, and A. J Chorin. Limitations of polynomial chaos expansions in the Bayesian solution of inverse problems. *Journal of Computational Physics*, 282:138–147, 2015.
- [21] Y. M. Marzouk and H. N. Najm. Dimensionality reduction and polynomial chaos acceleration of Bayesian inference in inverse problems. *Journal of Computational Physics*, 228(6):1862–1902, 2009.
- [22] Y. M. Marzouk, H. N. Najm, and L. A. Rahn. Stochastic spectral methods for efficient Bayesian solution of inverse problems. *Journal of Computational Physics*, 224(2):560–586, 2007.
- [23] Y. M. Marzouk and D. Xiu. A stochastic collocation approach to Bayesian inference in inverse problems. *Communications in Computational Physics*, 6:826–847, 2009.
- [24] X. Meng and G. E. Karniadakis. A composite neural network that learns from multi-fidelity data: Application to function approximation and inverse pde problems. *arXiv preprint arXiv:1903.00104*, 2019.
- [25] B. Peherstorfer, K. Willcox, and M. Gunzburger. Survey of multifidelity methods in uncertainty propagation, inference, and optimization. *SIAM Review*, 60(3):550–591, 2018.
- [26] M. Raissi, P. Perdikaris, and G. E. Karniadakis. Physics-informed neural networks: A deep learning framework for solving forward and inverse problems involving nonlinear partial differential equations. *Journal of Computational Physics*, 378:686–707, 2019.
- [27] P. Ramachandran, B. Zoph, and Q. Le. Searching for activation functions. *arXiv preprint arXiv:1710.05941*, 2017.
- [28] C. Schwab and J. Zech. Deep learning in high dimension: Neural network expression rates for generalized polynomial chaos expansions in uq. *Analysis and Applications*, 17(01):19–55, 2019.
- [29] A. M. Stuart. Inverse problems: a Bayesian perspective. *Acta Numerica*, 19(1):451–559, 2010.
- [30] A. M Stuart and A. Teckentrup. Posterior consistency for Gaussian process approximations of Bayesian posterior distributions. *Mathematics of Computation*, 87(310):721–753, 2018.
- [31] T. Tieleman and G. Hinton. Lecture 6.5-rmsprop: Divide the gradient by a running average of its recent magnitude. *COURSERA: Neural networks for machine learning*, 4(2):26–31, 2012.
- [32] R. K. Tripathy and I. Bilonis. Deep UQ: Learning deep neural network surrogate models for high dimensional uncertainty quantification. *Journal of Computational Physics*, 375:565–588, 2018.
- [33] Z. Wang, J. M. Bardsley, A. Solonen, T. Cui, and Y. M. Marzouk. Bayesian inverse problems with l₁ priors: A randomize-then-optimize approach. *SIAM Journal on Scientific Computing*, 39(5):S140–S166, 2017.
- [34] Z. Wang, T. Cui, J. Bardsley, and Y. Marzouk. Scalable optimization-based sampling on function space. *arXiv preprint arXiv:1903.00870*, 2019.
- [35] L. Yan and L. Guo. Stochastic collocation algorithms using l₁-minimization for Bayesian solution of inverse problems. *SIAM Journal on Scientific Computing*, 37(3):A1410–A1435, 2015.
- [36] L. Yan and Y. X. Zhang. Convergence analysis of surrogate-based methods for Bayesian inverse problems. *Inverse Problems*, 33(12):125001, 2017.
- [37] L. Yan and T. Zhou. An adaptive multi-fidelity pc-based ensemble Kalman inversion for inverse problems. *arXiv:1809.08931, to appear in International Journal for Uncertainty Quantification*, 2019.
- [38] L. Yan and T. Zhou. Adaptive multi-fidelity polynomial chaos approach to Bayesian inference in inverse problems. *Journal of Computational Physics*, 381:110–128, 2019.
- [39] M. Zeiler. Adadelta: an adaptive learning rate method. *arXiv preprint arXiv:1212.5701*, 2012.

- [40] Y. Zhu and N. Zabaras. Bayesian deep convolutional encoder–decoder networks for surrogate modeling and uncertainty quantification. *Journal of Computational Physics*, 366:415–447, 2018.